

Microwave reflection technique for electron cloud density measurement

H. Wang^a, J. C. Thangaraj^b, B. Zwaska^b, C. Y. Tan^c, B. J. Fellenz^c

^aMount Holyoke College, 50 College Street, South Hadley, Massachusetts 01075

^bAccelerated Physics Center, Fermi National Accelerator Laboratory, Batavia, Illinois 60510

^cAccelerator Division, Fermi National Accelerator Laboratory, Batavia, Illinois 60510

Abstract

The main challenge for the next generation high intensity proton beam transport is the formation of electron cloud. Microwave phase shift measurement has been a key diagnostic to measure e-cloud density. Direct phase shift measurement suffers from interference signals due to reflections from beamline components, leading to unlocalized phase shift. Recently, a method to enhance the phase shift by installing reflectors was proposed. In this paper, we report our first measurements on implementing microwave measurement based on reflection on an experimental setup. Dielectric thickness, location and spatial profile were varied and the effect on phase shift is described. The effect of end cap aperture length on phase shift measurement is also reported. A factor of 2-3 enhancement in phase shift is observed at certain frequencies.

Keywords: , electron cloud, microwave technique, dielectric, reflection, phase shift, electron cloud density, resonance, ears

1. Introduction

Project X is a multi-megawatt proton facility planned for construction at Fermilab. To achieve this goal, high current proton beam will have to be transported through the main injector [1]. The main injector is a synchrotron that accelerates 53 MHz proton bunches from 8 GeV to 120-150 GeV. During the passage of a high intensity proton bunch, low energy background electrons can interact with the proton bunch and develop instabilities. This could potentially limit the performance of the accelerator by increasing the vacuum pressure, emittance growth, shifting the tune of the machine among other things. Hence it is important to measure, model and mitigate electron cloud in such machines.

By sending EM waves through an electron cloud of uniform distribution and measuring the phase shift of the EM waves, the electron cloud density can be measured. The phase shift of an electromagnetic wave of frequency through an uniform, cold plasma (of plasma frequency and density) per unit length is given by [2]:

$$\frac{\varphi}{L} = \frac{\omega_p^2}{2c\sqrt{\omega^2 - \omega_c^2}}; \omega_p^2 = 4\pi\rho r_e c^2 \quad (1)$$

where c is the speed of light, r_e is the classical electron radius, and ω_c is the cut-off frequency of the pipe. The above formula assumes that the e-cloud density is static but in the main injector and other machines, the e-cloud density varies as a function of time. The reason being the proton bunch which generates the electron cloud has a time pattern. Hence, the e-cloud density varies as a function of time. So, sending a carrier wave into the cloud should result in a phase-modulation of the carrier

wave. In other words, in frequency spectrum, we expect to see sidebands to the carrier [3]. By measuring the amplitude of the sideband, in theory, we can estimate the electron cloud density.

Previous work on e-cloud measurements at Fermilab has focused on direct phase shift measurement with and without absorbers. When done without absorbers, the phase shift signal suffered from reflection from other parts of the machine and hence the measurement was not localized. When done with absorbers, though, the phase shift signal was very low [4][5]. Our aim in this work was to make the measurement both localized and increase the signal amplitude. We do this by installing reflectors on the beam pipe. By deliberately installing reflectors, we can control the reflections and thereby increase the signal and make it localized at the same time [6]. This paper reports our experimental measurements on the study of microwave reflection for the specific case of the Fermilab Main injector beam pipe for various dielectric thickness, orientation and location for different sets of antenna. We begin by describing the experimental setup and then discuss the experimental methods we undertake. Next, we discuss the results of the measurement and end with our conclusion and future work.

2. Experimental Setup

The schematic graph of the experiment is shown in Figure 1. We used an Agilent E5071C (9 kHz - 8.5 GHz) ENA Series Network Analyzer (1) to generate and analyze the electromagnetic wave propagating in the main injector waveguide (5). The steel elliptical waveguide had a longitudinal dimension of 1.01 m. In the cross section, its dimension was 12.065 cm by 5.4 cm. The port 1 and port 2 of the network analyzer were coupled to a transmitter (2) and a receiver (3) antennas through coaxial cables. The distance between the antenna and the corresponding

Email address: wang24h@mt holyoke.edu (H. Wang)

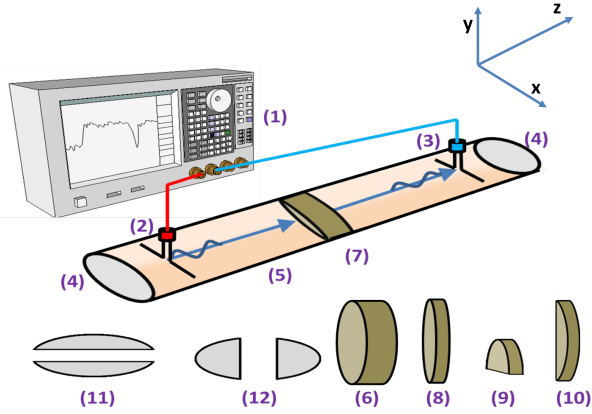


Figure 1: Experimental setup schematic view. Here are: (1)–Agilent network analyzer; (2)–transmitter antenna; (3)–receiver antenna; (4)–metal reflectors; (5)–steel main injector waveguide; (6)–2.54 cm thick Teflon dielectric; (7)–1.27 cm thick Teflon dielectric; (8)–0.44cm thick Teflon dielectric; (9)–1.27cm thick half sized 'short' dielectric; (10)–1.27 cm thick half sized 'long' dielectric; (11)–'ear' reflector along long axis; (12)–'ear' reflector along short axis.

end of the waveguide is 5.08 cm. Teflon dielectrics (6, 7, 8, 9, 10) were used to investigate the effects of electron cloud on the phase of the propagating wave. The dielectrics were of three different thickness: for (6), (7) and (8), the thickness was 2.54 cm, 1.27 cm and 0.44 cm, respectively. Meanwhile, half-sized dielectrics were also designed, with (9) cut along y -axis and (10) along x -axis. Both (9) and (10) were 1.27 cm in thickness. The waveguide with an open-boundary can be converted to a closed-boundary cavity by closing the pipe with two metal reflectors (4) at the both ends. The reflectors were cut along the x -axis (11) or the y -axis (12), with gap distance varying from 0.635 cm to 10.795 cm for (12), or from 0.95 cm to 3.49 cm for (11).

3. Experimental Methods

The experiment was done in two stages: the first stage was to test the performance of various designs of antennas, and to compare the waveguides with either an open or a closed boundary; the second stage was to investigate the phase shift dependence on various factors, including dielectrics and reflectors.

3.1. Antenna testing method

We tested in total 9 half-wave dipole antennas with single arm length ranging from 2.54 cm to 5.08 cm, and 10 quarter-wave vertical antennas with arm length between 1.27 cm and 4.13 cm. All antennas were soldered and positioned in the xy -plane of the waveguide throughout the measurements, as shown in Figure 1. The frequency was swept from 1 GHz to 4 GHz using the network analyzer. We focused on the S21 parameter of the network analyzer and recorded the trace data of both S21 and S11 in the power log format. S21 parameter describes how much is transferred from port 1 to port 2 of the network analyzer; S11 parameter, on the other hand, describes how much power is reflected back to port 1, therefore it can be used as a

measure of the power transmission in the waveguide. We conducted S21 measurements with both the open boundary waveguide and the closed boundary cavity. After powering on the network analyzer, transverse electromagnetic (TE) wave traveled in the waveguide/cavity from the transmitter (2) to the receiver (3), and then displayed on the front panel of the network analyzer. We conducted data analysis of the trace data, and investigated the S21 power log format result for the waveguide and the cavity. The same process was repeated for every type of antennas, during which we made sure that the only variable was the change of antennas.

3.2. Phase shift measurement methods

We placed dielectrics within the waveguide and the cavity to measure the phase shift caused by the dielectrics. To ensure the accuracy in phase measurements, we calibrated the two cables connecting the network analyzer to the antennas by directly putting the two connectors together. Then, a 'THRU' calibration was conducted using the network analyzer calibration kit, which can kill the extra phase shift caused by the cables at high frequencies. We used the expand phase format of the Agilent network analyzer, which can display phase beyond the $\pm\pi$ limit of the normal phase format found in most network analyzers.

To obtain the *phase shift* without reflection, we first measured the expand phase of the TE wave in an open waveguide. Then, we inserted the dielectric and measured the expand phase of the microwave signal in the waveguide. By subtracting the set of phase data without dielectric from the set with dielectric, we obtained the *net phase shift* due to the dielectric alone without reflection. We repeated the same process with the closed boundary cavity to get the *net phase shift* with the reflection. A comparison between the two setups was also drawn and analyzed.

The effect of dielectric location, dielectric thickness, and dielectric spatial profile was also studied. In all of the following description of experiment, we kept the boundary closed with reflectors.

For the study of the dielectric location, we used the 2.54 cm dielectric and placed it at three different locations: center, one third and one fourth of the cavity. A 22.88 cm measuring stick with length markings was employed to guarantee that the dielectric stay in the exact desired location. For each different location of the dielectric, *net phase shift* data was obtained by subtracting the phase of the microwave signal without the dielectric from that with the dielectric, with a span of frequency from 1.5 GHz to 3 GHz.

Dielectrics of different thickness were later put in the center of the cavity separately: 5.08 cm, 2.54 cm and 1.44 cm. The measurement to extract *net phase shift* was repeated for each dielectric thickness. We also tested how the dielectric distribution profile could affect the phase shift measurement. Two identical 1.27 cm dielectrics were cut along the short or long axis, therefore *short half-sized* dielectric or *long half-sized* dielectric. For each half-sized dielectric, *net phase shift* was calculated with the closed boundary.

Finally, we tested phase shift dependency on end aperture geometry of the originally closed boundary (4). We systemati-

cally varied the orientation of the aperture – horizontal (11) or vertical (12) – and the frequency of the exciting field (from 1.5 GHz to 3 GHz), and measured the reflection coefficient S_{21} as well as the expand phase for these settings. Both transmission and *net* phase shift for all the settings were calculated. Once again, we emphasized that net phase shift means subtracting the phase of the one data set with dielectric from the phase of another data set without the dielectric.

4. Results and discussion

4.1. Antenna testings

Antennas are widely used for transmitting radio-frequency signals. They are able to couple the currents that are flowing in the wires into electromagnetic waves in the waveguide. As shown in Figure 2, two antenna designs were tested: dipole antenna and monopole antenna, the former regarded as the most basic and practical antenna design [7].

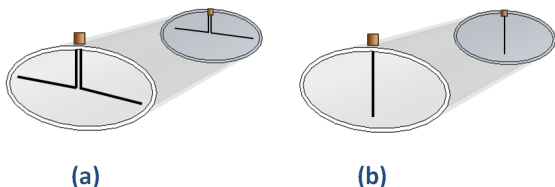


Figure 2: Schematic graph of a dipole antenna (a) and a monopole antenna (b) in the cross section of the elliptical waveguide.

A dipole antenna shown in Figure 2 (a) is composed of two simple metal wires, parallel and in line with each other, with a small space acting as the center-fed driven element between the two conductors. When a voltage is applied to the antenna at the center, current flows in the wires and builds up electrical charges in either end of the conductors, similar to a dipole moment separated by the distance between the two ends. As the center-fed voltage alternates, the dipole moment (the current) oscillates across the antenna, creating oscillating electric and magnetic fields that propagate outward. The orientation of the created electric field is along the axis of the antenna, with the magnetic field perpendicular to both the electric field and the direction of propagation. Meanwhile, as the electromagnetic wave generated by the transmitter passes over the conducting wires of the other dipole antenna, an oscillating current will be induced as a result.

Efficiency of an antenna is defined as the ratio of power radiated in all directions to the power absorbed by the terminals. Lowering the efficiency will result in less power radiated from the antenna. Impedance mismatch between the transmitter and receiver will also cause antenna loss. To ensure the impedance match, dipole antenna with the total length slightly less than half of the ideal carrier wavelength is used (half-wave dipole). When fed with a radio-frequency current at the resonant frequency, a standing wave will form along the half-wave dipole wires with the peak current at the feedpoint. Using this design,

we can obtain a more efficient and appropriate matching antenna network [7]. Even though a dipole antenna needs to be used at the resonant frequency to work more efficiently, it can still transmit signals with frequencies far from the resonant frequency. In this case, impedance mismatch results in antenna loss.

Monopole antenna shown in Figure 2 (b) with the total length equal to one arm of a half-wave dipole is also regarded as the more efficient resonant antenna design (quarter-wave monopole). The other arm of the half-wave dipole is replaced by a connection to a ground plane, which, in our experiment, would be the conductor wall of the waveguide. Though the design of a quarter-wave monopole is simpler than a half-wave dipole, the power radiated by a quarter-wave monopole is roughly half the power radiated by a dipole. Meanwhile, in order to achieve resonance for a quarter-wave monopole, the required length is beyond the physical geometry of the elliptical waveguide. Nonetheless, we tested both the dipole and monopole antenna designs and compared the resonant peak for each model.

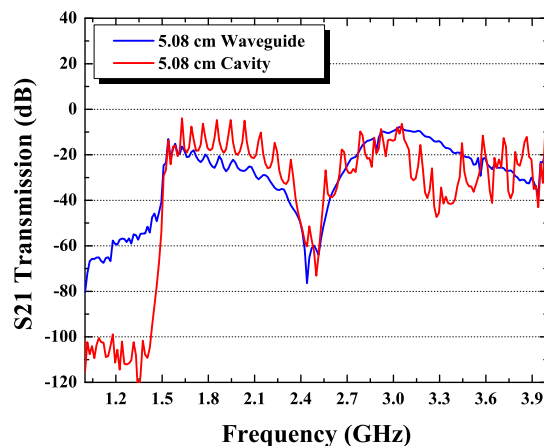


Figure 3: S_{21} transmission for dipole antennas with one arm length of 5.08 cm in a 1.01 m main injector waveguide (blue) and cavity (red) with a cutoff frequency of 1.52 GHz.

Results of the S_{21} transmission for the half-wave dipole with one arm length of 5.08 cm are shown in Figure 3. Both the cavity with closed boundary and the waveguide with open boundary were presented in the frequency domain from 1 GHz to 4 GHz. At frequency lower than 1.52 GHz, the transmitted power for both the waveguide and the cavity are very small compared to the incident power, indicating a frequency threshold below which the electromagnetic wave cannot propagate. This frequency is defined as the cutoff frequency of the waveguide, which is the cutoff frequency of the lowest propagating mode. The cutoff frequency of a waveguide is determined by the cross section geometry of the waveguide: the length of the long axis and the short axis. For the test elliptical waveguide, the lowest propagating mode is the even TE₁₁ mode, with a cutoff frequency at around 1.49 GHz [10]. Even TE₁₁ mode can be excited by a half-wave dipole positioned along the long axis with the resonant frequency of around 1.49 GHz. Therefore, the dipole with one arm length of around 5.03 cm would be best coupled to the even TE₁₁ mode. As the dipole arm

length decreases, antenna loss increases.

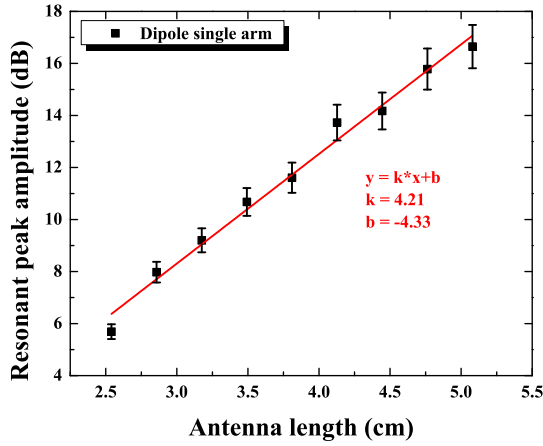


Figure 4: Resonant frequency peak amplitude for dipole antennas with different dipole single arm length, in closed boundary waveguide.

As the boundaries were closed by the metal end caps, reflections occurred in the cavity, whose presence is indicated by the resonant frequency peaks in Figure 3. The waveguide also showed some resonance, though to a much lesser degree compared to the cavity, because a finite waveguide also possesses a boundary that could cause reflections. The amplitude of the resonant frequency peak decreases as the dipole single arm length decreases, as seen in Figure 4, indicating again the antenna loss caused by impedance mismatching.

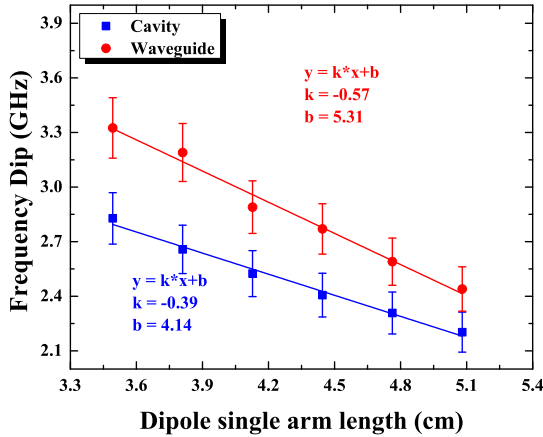


Figure 5: Plot of the frequency of the S21 transmission dip with regard to the length of dipole single arm, for both open boundary waveguide and closed boundary cavity.

Also present in Figure 3 is an obvious S21 transmission dip at approximately 2.5 GHz for the 5.08 cm dipole. As the dipole single arm length decreased from 5.08 cm to 2.54 cm, the frequency of the transmission dip increased linearly (Figure 5), suggesting a correlation between the antenna design and the transmission dip. In fact, the dip was caused by the power loss of the dipole at the center fed element [7]. All further measurements avoided the frequency range of the transmission dip as antennas performed poorly.

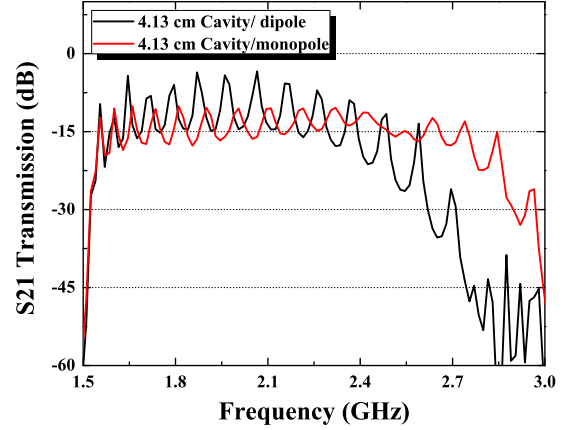


Figure 6: S21 transmission for both the dipole and monopole antennas in a closed boundary cavity. Network analyzer swept frequency from 1.5 GHz to 2.4 GHz

Figure 6 plots the S21 transmission for the dipole and monopole, both positioned in the closed boundary cavity, with regard to frequency between 1.5 GHz and 2.4 GHz. Cutoff frequency was unchanged as well as the presence of the resonance, yet the amplitude of the resonant frequency peak when using the dipole antennas was larger than that when using the monopole antennas. The decrease in resonance amplitude corresponded to monopole antenna's lesser radiated power even with the same input [8].

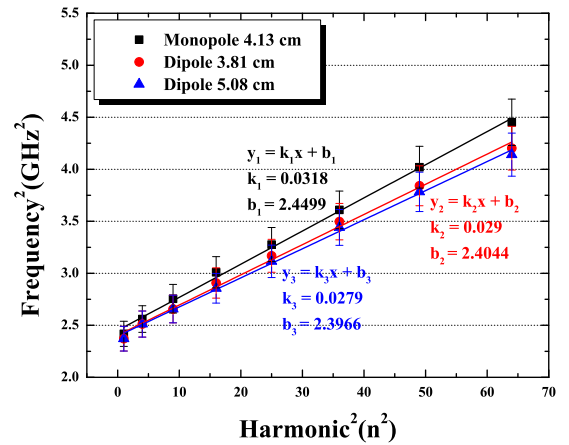


Figure 7: Linear dependency of harmonic frequencies, f^2 , on harmonic number, n^2 . Three antenna designs were tested: (a) monopole antenna with arm length 4.13 cm, (b) dipole antenna with one arm length 3.81 cm, (c) dipole antenna with one arm length 5.08 cm.

Harmonics are indications of the standing waves in the cavity. The formation of the standing wave requires that the longitudinal dimension of the beam pipe is a multiple of the half-wavelength of the resonant frequency. Using the dispersion relation in a waveguide, the frequency f of the n th resonant harmonic satisfies the hyperbolic relationship [9]

$$f^2 = \frac{c^2}{4L^2}n^2 + f_c^2. \quad (2)$$

Value of f for each n th resonant harmonic can be extracted from

| | 5.08 cm dipole | 3.81 cm dipole | 4.13 cm monopole |
|------------------------|-------------------|-------------------|---------------------|
| Calculated L (cm) | 89.7 | 88.1 | 84.1 |
| Measured L (cm) | 91.4 | 91.4 | 91.4 |
| Calculated f_c (GHz) | 1.54 | 1.54 | 1.54 |
| Measured f_c (GHz) | 1.52 | 1.52 | 1.52 |

Table 1: Comparison between calculated length L and measured L , calculated cutoff frequency f_c and measured f_c , for three antenna designs: (a) 5.08 cm dipole antenna, (b) 3.81 cm dipole antenna, (c) 4.13 cm dipole antenna. The measured length L refers to the length between the two antennas.

Figure 3. Instead of plotting f with regard to n , we showed in Figure 7 that f^2 linearly depended on n^2 , for all the three antenna designs. Linear fitting was applied to the three data set, from which we were able to obtain the individual slope $\frac{c^2}{4L^2}$ and intercept f_c^2 . Furthermore, we could calculate the experimental values of the total length L of the beam pipe as well as the cutoff frequency f_c , and compared the calculated values with the actual length L or the measured f_c (1.52 GHz). The calculated and measured values are shown in the table (Table 1) below.

As shown in Table 1, 5.08 cm dipole, which is the half-wave dipole for fundamental mode even TE₁₁, showed the best agreement with the actual measured length 91.4 cm. Comparing L for the 3.81 cm dipole and 4.13 cm monopole, the shorter dipole gave a better approximation of the actual length than the longer monopole. This further confirmed the assumption that dipole antennas with longer length are the optimal choice for signal transmission. The difference between the calculated and measured cutoff frequency is minimal, at approximately 0.02 GHz. For different antenna design, neither the calculated f_c nor the measured f_c changed, in good accordance with the fact that cutoff frequency depends on the physical geometry, not the transmitting or receiving antenna.

4.2. Phase shift measurements

Using the optimal antenna design (5.08 cm half-wave dipole) demonstrated before, we measured the net phase shift caused by the Teflon dielectric ($\epsilon_r = 2.03$) based on various conditions, including the dielectric location, dielectric thickness, dielectric spatial distribution profile, and the end aperture geometry.

Reflections can increase the phase shift signal by increasing the total effective length of the dielectric, especially at resonant frequencies where standing waves are formed [6]. Figure 8 is composed of two parts: the top describes the difference in frequency spectrum due to the insertion of the dielectric (dielectric was positioned at the center of the waveguide); the bottom illustrates the difference in the net phase shift due to the reflections. The increase in net phase shift can be easily seen comparing the phase shift peaks with or without the reflections. At approximately 2.25 GHz, the ratio between the two phase shifts reaches 2.42. However, the effect of reflections is not always the case for all S₂₁ transmission resonant frequencies. The bigger frequency shift in S₂₁ transmission lined up perfectly with the peak in net phase shift, as shown in Figure 8. Similarly, when the harmonics showed no frequency shift, the corresponding

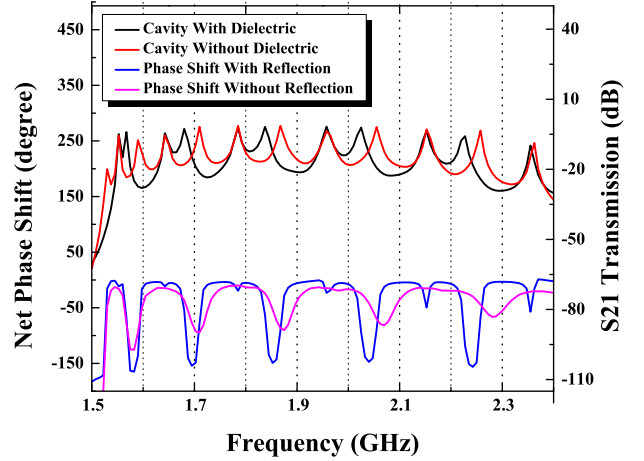


Figure 8: **Top**: S₂₁ Transmission in the closed-boundary-waveguide with (black) or without (red) dielectric from 1.5 GHz to 2.4 GHz. **Bottom**: the phase shift due to the dielectric for both an open-boundary-waveguide (magenta) and a closed-boundary waveguide (blue).

phase shift was at the node. This can be explained by changing the location of the dielectric. Instead of putting the 2.54 cm dielectric at one half of the cavity, it was positioned at one third or one fourth of the cavity length. The net phase shift for each position is shown in Figure 9 - 11.

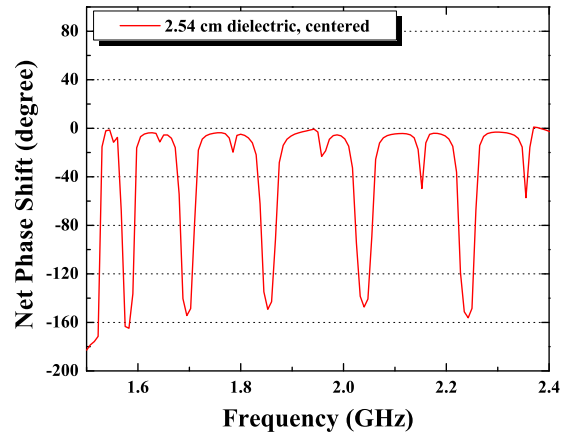


Figure 9: Net phase shift due to a 2.54 cm dielectric from 1.5 GHz to 2.4 GHz with the dielectric positioned at the center of the closed boundary waveguide.

Since the frequency was swept from 1.5 GHz to 3 GHz, approximately 10 to 20 half wavelengths could fit in the cavity, respectively. When the dielectric was at the center of the cavity, it was also at the node of the standing waves with the even harmonic numbers: 10, 12, 14, 16, 18, 20. Therefore, for those standing waves, the dielectric was 'invisible', inducing no phase shift (Figure 9). For those with the odd harmonic numbers (11, 13, 15, 17, 19), the dielectric sat at the anti-node of each standing wave, corresponding to the peak in net phase shift. The node in net phase shift plot would, as a consequence, repeat every other peak (Figure 9).

Similarly, when the dielectric was located at one third of the cavity length, it was also at the node of every other two harmonics. Otherwise, phase shift would occur when the dielectric

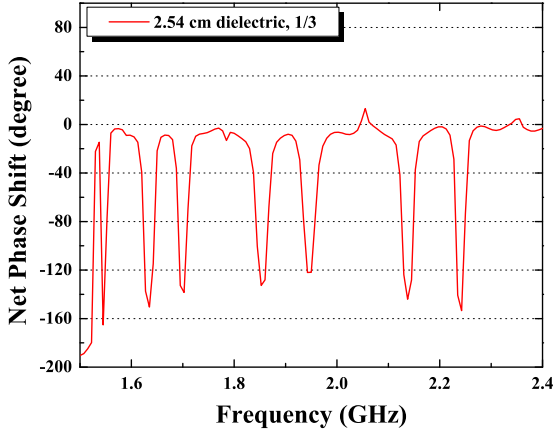


Figure 10: Net phase shift due to a 2.54 cm dielectric from 1.5 GHz to 2.4 GHz with the dielectric positioned at one third of the closed boundary waveguide.

was located at the non-node of the rest of the harmonics. Consequently, the node in net phase shift would repeat every other two peaks (Figure 10). The same behavior could be observed in the case when the dielectric was positioned at one fourth of the cavity length, when the node repeated every other three peaks (Figure 11).

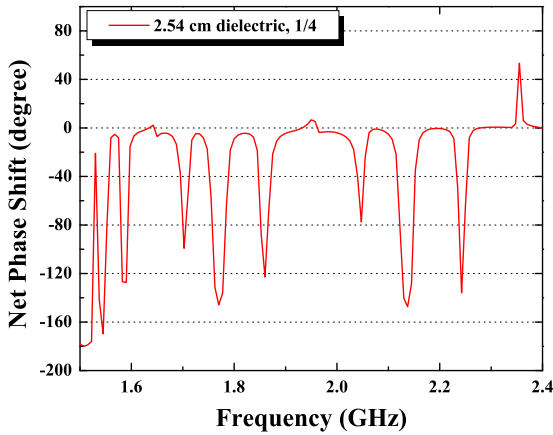


Figure 11: Net phase shift due to a 2.54 cm dielectric from 1.5 GHz to 2.4 GHz with the dielectric positioned at one fourth of the closed boundary waveguide.

Dielectric thickness also characterizes the phase shift measurement. Figure 12 plots the net phase shift for three different thickness: (a) 5.08 cm, (b) 2.54 cm, (c) 1.44 cm. As the dielectric thickness increased from 1.44 cm to 5.0 cm, overall the net phase shift consistently increased, indicating the increase in effective dielectric length. Comparing the peak net phase shift increase to that for the nodes, the latter showed bigger increase at higher frequency, as the wavelength became relatively smaller compared to the dielectric. Therefore, the dielectric was at the node of the standing waves, it became visible again to high frequency waves.

In the actual main injector, the electron distribution in electron cloud will also affect the phase shift measurement. Thus characterizing dielectric spatial distribution profile on net phase shift is also crucial for the purpose of our measurement. As seen

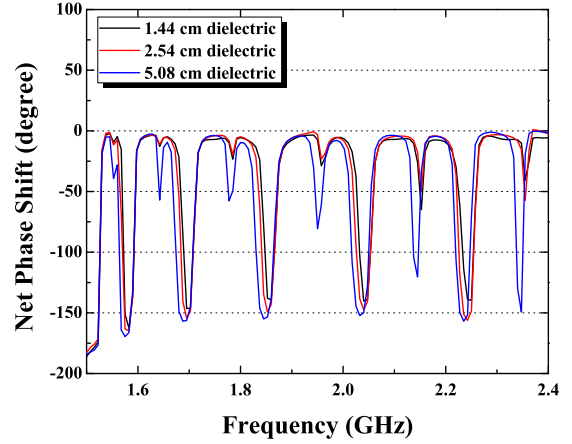


Figure 12: Net phase shift in the closed-boundary-waveguide from 1.5 GHz to 2.4 GHz due to the whole-sized-dielectric with three different thickness: (a) 5.08 cm dielectric (blue), (b) 2.54 cm dielectric (red), (c) 1.44 cm dielectric (black).

in Figure 13, three dielectric spatial profiles were tested: the whole sized elliptical dielectric and two half sized dielectrics each cut along either the long or short axis. The whole dielectric (red) apparently induced more phase shift than the two half sized (black and blue), as expected, though only to a small ratio (1.27) considering that the size ratio is 2. The two different half sized dielectrics displayed no big difference in net phase shift, particularly at lower frequencies, because of the symmetric electric field line distribution in the elliptical waveguide [10].

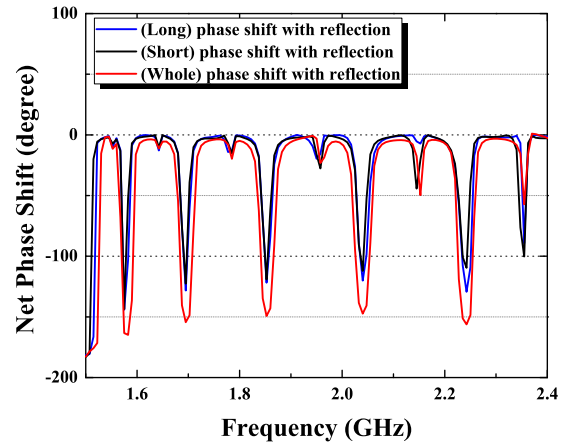


Figure 13: Net phase shift in the closed-boundary-waveguide from 1.5 GHz to 2.4 GHz due to the 1.27 cm dielectric with three different spatial profiles: the whole-sized-dielectric (red), the half-sized-long-dielectric (blue) and the half-sized-short-dielectric (black).

Another difference between the actual experimental scenario in the main injector and the testing waveguide is that the former requires an opening in both ends so that the proton beam particles to go through. As a result, we systematically altered the end aperture geometry to monitor how the phase shift measurement would change. As the end aperture increases, more electric field lines will escape from the opening, resulting in less reflections.

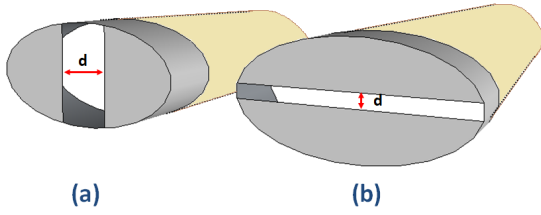


Figure 14: Schematic for the two end cap designs: (a) short ears, (b) long ears.

Since reflections can enhance the phase shift measurements, we tried to maximize the net phase shift while at the same time ensuring the end opening was wide enough, otherwise the latter could act as a protrusion to the proton beams.

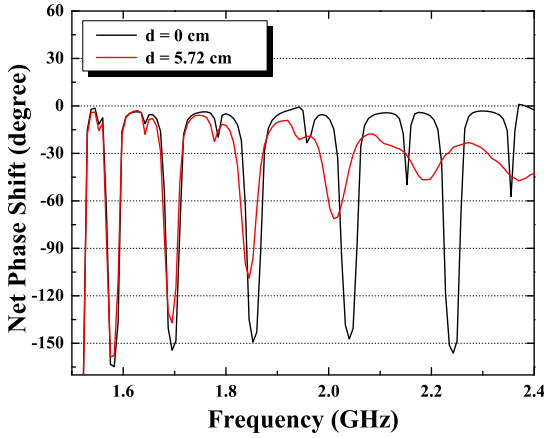


Figure 15: Net phase shift between 1.5 GHz to 2.4 GHz due to the 2.54 cm dielectric with 5.72 cm *short* end aperture and closed cavity.

Figure 15 shows the net phase shift at frequencies between 1.5 GHz to 2.4 GHz with the 2.54 cm dielectric centered in the cavity. As the cavity changed from being entirely enclosed by the metal end caps to partially closed with a 5.72 cm opening along the short axis, which was around 47% of the cross section, net phase shift decreased based on different frequency range. Higher frequencies saw a bigger decline in phase shift, because their shorter wavelengths made it easier to escape the 47% opening of the cross section. At frequencies closer to the cutoff frequency, their wavelength was substantially larger than the opening space, therefore few waves managed to escape the cavity, retaining the reflections that enhanced the phase shift. Meanwhile, according to the phase shift equation (without reflection) [9]

$$\Delta\Phi = \frac{n_e e^2 L}{4\pi c \epsilon_0 m_e \sqrt{f^2 - f_c^2}}, \quad (3)$$

the closer the frequency f to the cutoff f_c , the bigger the phase shift $\Delta\Phi$. So the phase shift at lower frequencies closer was increased not only by the retained reflections but also being closer to the cutoff frequency. This made the lower frequencies the optimal range to measure the phase shift.

Figure 17 plots the the net phase shift for each *phase* harmonic with regard to frequency, for all the short end aperture

geometry as d ranged from 0 cm (completely closed) to 12.07 cm (completely open). This plot showed two transitions in phase shift as the opening increased. When the end aperture increased from 0 cm to 3.18 cm (26% of the cross section), minimal change in net phase shift occurred for all phase harmonic peaks, suggesting the small effect of the opening on phase shift measurements. As the opening increased further to 6.99 cm (58% of the cross section), phase shift at higher frequencies first started to decrease, though the phase shift for the first two harmonic peaks still remained rather close to that for the entirely closed cavity (74% for the second phase harmonic, 93% for the first phase harmonic). In this case, as described before, high frequencies started to leak form the cavity, diminishing the enhancing effect of the reflections. Finally, as the opening increased to 12.07 cm, the phase shift for each phase harmonic started to increase again, though the frequencies closer to the cutoff frequency still displayed bigger phase shift values, in good accordance with Eqn. 3. Further analysis on the boundary conditions is needed to better explain the behavior during the third stage.

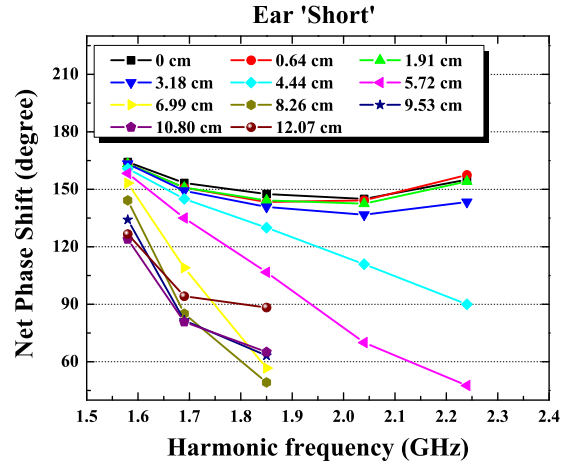


Figure 16: Net phase shift of the first five harmonic frequencies with different *short* end aperture geometry (d = length of the aperture) : (a) $d = 0$ cm, (b) $d = 0.64$ cm, (c) $d = 1.91$ cm, (d), $d = 3.18$ cm, (e) $d = 4.44$ cm, (f) $d = 5.72$ cm, (g) $d = 6.99$ cm, (h) $d = 8.26$ cm, (i) $d = 9.53$ cm, (j) $d = 10.80$ cm, (k) $d = 12.07$ cm.

Another end aperture geometry was also studied: the long end aperture. The difficulty to construct clean opening along the long axis is shown in Figure 18, as the phase shift at some frequencies demonstrated irregular behavior. However, we could still observe that as the opening distance d increased from 0 cm to 2.22 cm (41% of the cross section), the decrease in phase shift arose. Similar to the short axis end aperture, higher frequencies exhibited bigger phase shift decrease. The phase harmonics closer to the cutoff frequency also displayed bigger phase shift as expected.

Figure 17 shows the net phase shift for each phase harmonic with regard to frequency, for all the long end aperture d . Instead of observing three stages of phase advance, we saw a more uniform decrease in phase across all frequencies as d increased, and the amplitude of decrease was bigger than that with the

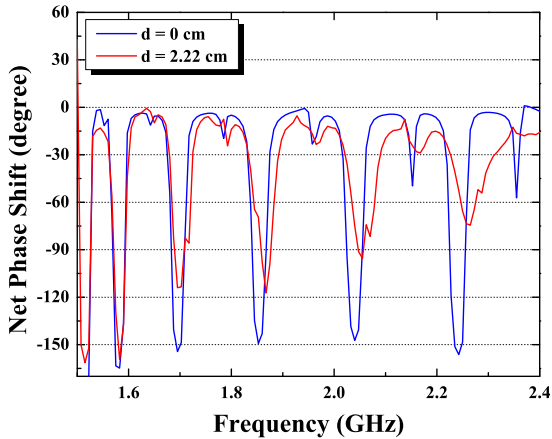


Figure 17: Net phase shift between 1.5 GHz to 2.4 GHz due to the 2.54 cm dielectric with 2.22 cm long end aperture and closed cavity.

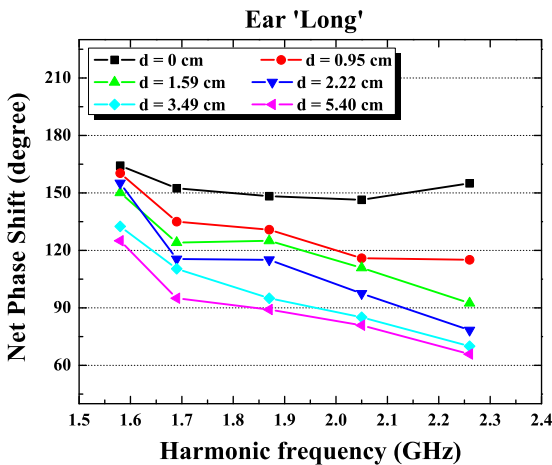


Figure 18: Net phase shift of the first five harmonic frequencies with different long end aperture geometry (d = length of the aperture) : (a) $d = 0$ cm, (b) $d = 0.95$ cm, (c) $d = 1.59$ cm, (d) $d = 2.22$ cm, (e) $d = 3.49$ cm, (f) $d = 5.40$ cm.

short end aperture. For example, as the end aperture increased from 0% to around 45% (approximately 5.72 cm for the short aperture, 2.22 cm for the long aperture), the second phase harmonic was decreased by 12% for the short aperture (Figure 16), and by 25% for the long aperture (Figure 18).

Comparing the results of net phase shift with a long end aperture geometry to a short end aperture, we could see a smaller net phase shift spread as d changed along the long axis, which would make this end aperture design an optimal choice if a bigger frequency range is desired. However, if the frequency range for measuring phase shift is rather close to the cutoff frequency of the waveguide, the short end aperture gives a bigger phase shift value. However, the nature of the effects of ears on reflections is unclear, and further investigation is required to fully understand their effects.

5. Conclusions

We have demonstrated the phase shift enhancement due to the reflections inside the waveguide. We have analyzed dif-

ferent antenna configurations, dielectric location, thickness and spatial profile. We also have measured the effect of end cap gap on the phase shift measurements. Initial experimental studies indicate that there could be a possible advantage by putting ears in the beam pipe. But it also depends on the frequency range of interest. For example, at higher frequency range, the long ears give a bigger phase shift compared to the short ears, while at lower frequency range close to the cutoff, the short ears display bigger phase shift. Our experiment also explains the role of reflection on phase shift measurement and other observations [9]. As discussed before, reflection enhances the phase shift measurement by up to a factor of 3 at some resonant harmonics. For other resonant harmonics, reflection shows little enhancement effect. This behavior is explained by positioning the dielectric at various locations of the waveguide.

6. Future work

Further study on characterizing the boundary conditions when using ear reflectors is needed to fully understand their effect on phase shift measurement. Careful analysis of the field distribution of various modes in the elliptical waveguide along with efficient antenna design and polarization is also essential to characterize the effect.

7. Acknowledgment

We thank Ioanis Kourbanis for supporting e-cloud work, and Nathan Eddy for his thoughts on the beam pipe setup. We also thank E. Harms and T. Koeth for their assistance and encouragement.

References

- [1] I. Kourbanis et al., "Current and Future High Power operation of Fermilab Main Injector", Fermilab Note, Fermilab-conf-09-151-ad, 2009.
- [2] K. Sonnad et al., "Simulation and Analysis of Microwave transmission through an electron cloud a comparison of results", Proceedings of PAC'07, 2007.
- [3] F. Caspers et al., "The CERN SPS experiment on microwave transmission through the beam pipe", Proceedings of PAC'05, 2005.
- [4] J. Crisp et al., "Measurement of electron cloud density with microwaves in the Fermilab main injector", DIPAC'09 Basel, Switzerland TUPB23; <http://www.JACoW.org>.
- [5] J. Thangaraj et al., "Electron Cloud Studies in the Fermilab Main Injector using Microwave Transmission", ECLLOUD 2010, Ithaca, New York; USA.
- [6] C. Tan "Measuring electron cloud density with trapped modes", Fermilab Note (unpublished).
- [7] Constantine A. Balanis "Antenna Theory: Analysis and Design", Wiley-Interscience, 3rd Edition, 2005.
- [8] Warren L. Stutzman, Gary A. Thiele, "Antenna Theory and Design", Wiley, 2nd Edition, 1997.
- [9] K. Hammond et al., "Effects of reflections on TE-wave measurements of electron cloud density", ECLLOUD 2010, Ithaca, New York; USA.
- [10] Nathan Marcuvitz "Waveguide Handbook", Institution of Electrical Engineers, London, 1986.